Active normal faulting during the 1997 seismic sequence in Colfiorito, Umbria: Did slip propagate to the surface?

Zoë K. Mildon[1.], Gerald P. Roberts[2.], Joanna P. FAURE WALKER[1.], Luke N. J. Wedmore[1.], Ken J. W. McCaffrey[3.]

1. Institute for Risk and Disaster Reduction, University College London, Gower Street, London, WC1E 6BT

2. Department of Earth and Planetary Sciences, Birkbeck, University of London, Malet Street, London, WC1E 7HX

3. Department of Earth Sciences, Durham University, Durham DH1 3LE

Corresponding author: Z.K. Mildon, Institute for Risk and Disaster Reduction, University College London, Gower Street, London, WC1E 6BT, zoe.mildon.13@ucl.ac.uk

Keywords: mechanics of faulting, tectonic geomorphology, active faulting, coseismic surface slip

Abstract

In order to determine whether slip during an earthquake on the 26th September 1997 propagated to the surface, structural data have been collected along a bedrock fault scarp in Umbria, Italy. These collected data are used to investigate the relationship between the throw associated with a debated surface rupture (observed as a pale unweathered stripe at the base of the bedrock fault scarp) and the strike, dip and slip-vector Previous studies have suggested the surface rupture was produced either by primary surface slip or secondary compaction of hangingwall sediments. Some authors favour the latter because sparse surface fault dip measurements do not match nodal plane dips at depth. It is demonstrated herein that the strike, dip and height of the surface rupture, represented by a pale unweathered stripe at the base of the bedrock scarp, shows a systematic relationship with respect to the geometry and kinematics of faulting in the bedrock. The strike and dip co-vary and the throw is greatest where the strike is oblique to the slip-vector azimuth where the highest dip values are recorded. This implies that the throw values vary to accommodate spatial variation in the strike and dip of the fault across fault plane corrugations, a feature that is predicted by theory describing conservation of strain along faults, but not by compaction. Furthermore, published earthquake locations and reported fault dips are consistent with the analysed surface scarps when natural variation for surface dips and uncertainty for nodal plane dips at depth are taken into account. This implies that the fresh stripe is indeed a primary coseismic surface rupture whose slip is connected to the seismogenic fault at depth. We discuss how this knowledge of the locations and geometry of the active faults can be used as an input for seismic hazard assessment.

1. Introduction

For seismic hazard assessment it is important to know the locations and geometries of active faults, as the proximity of a location to an active fault is a key factor that determines the predicted degree of shaking (e.g. *Roberts et al.*, 2004). There are some examples of seismic hazard assessment in different tectonic settings that use active fault traces as an input for probabilistic seismic hazard assessment (PSHA), notably the Uniform California Earthquake Rupture Forecast (UCERF, *Field et al.*, 2009), as well as PSHA for Taiwan (*Cheng et al.*, 2007) and New Zealand (*Stirling et al.*, 2002). In the central Italian Apennines an ongoing debate concerns the locations of active faults with one key issue being whether earthquake slip at depth propagates to the surface producing bedrock (carbonate) scarps preserved through the Holocene (*Roberts and Michetti*, 2004). Bedrock fault scarps are well exposed throughout this region, yet it is debated in the literature whether they should be considered active and forming due to coseismic slip (*Blumetti et al.*, 1993; *Michetti et al.*, 2000; *Schlagenhauf et al.*, 2010; *Vittori et al.*, 2011) or inactive and forming through geomorphic processes such as landslides (*Anzidei et al.*, 1999; *Cinti et al.*, 1999; *Chiaraluce et al.*, 2003). For example, the Database of Individual Seismogenic Sources (DISS; *Basili et al.*, 2008) does not use the surface traces of faults offsetting bedrock geology and/or Holocene slopes to delineate the locations and geometries of active faults. Instead fault traces are simplified into rectangles or boxes that encompass the locations of fault slip from historical earthquakes or those defined by palaeoseismology (see Figure 1). In contrast, other fault databases define fault locations and geometries using observations of offset bedrock geology and Holocene slopes (e.g. *Piccardi et al.*, 1999; *Galadini and Galli*, 2000; *Vittori et al.*, 2000; *Boncio et al.*, 2004; *Roberts and Michetti*, 2004; *Faure Walker et al.*, 2010). In this paper, we investigate a well-exposed bedrock scarp in Umbria associated with an earthquake in 1997 that shows evidence of surface ruptures to help resolve this controversy.

From September 1997 until April 1998 there was a prolonged seismic sequence in the Umbria region, centred on the town of Colfiorito (the mainshocks are shown in Figure 1). Earthquakes occurred over a north-west to south-east elongated zone approximately 40km long (*Amato et al.*, 1998; *Deschamps et al.*, 2000; *Ripepe et al.*, 2000). There were three mainshocks during the sequence with M_w>5.5; Event 1 at 00:33 on the 26th September 1997 (M_w=5.7), Event 2 at 09:40 on the 26th September 1997 (M_w=6.0) and Event 3 at 15:23 on the 14th October (M_w=5.6). Surface effects of the three mainshocks were widely recorded in the epicentral region immediately after the earthquakes occurred (*Basili et al.*, 1998; *Cello et al.*, 1998; *Vittori et al.*, 2000). Such effects included cracking of road and the ground surface, open fissures, alluvial scarps, landslides, and the appearance of a brown, soil-covered, stripe at the base of the bedrock scarp. This stripe is now visible as a pale unweathered stripe at the base of the MLS fault (Figure 1 and 2). A similar pale stripe can be observed along the north-west section of the CSM fault (Figure 1). There is some controversy regarding joining the surface observations to the first two main shocks. *Chiaraluce et al.* (2005) hypothesise that Event 1 occurred on the MLS fault. However according to the observations of the CSM fault before and after Event 2 (*Cello et al.*, 1998) the surface effects were the same, hence they associate Event 1 with the CSM fault. However when the earthquake hypocentre are plotted in relation to the surface expressions of the faults, Event 1 occurred almost directly beneath the CSM fault (Figure 1). This does not support Event 1 located on the CSM fault. One possibility is that Event 1 was a composite rupture of the MLS and CSM faults. Event 2 is also likely to be located on the MLS based on the hypocentre locations. Some authors argue that the stripe at the base of the fault scarp results from coseismic slip from a mainshock event (*Cello et al.*, 1998, 2000; *Vittori et al.*, 2000). In contrast, other authors argue that all surface effects are secondary (i.e. non-tectonic). *Cinti et al.*, 2000 argue for broad NW-SE zones of deformation, comprising of surface breaks and landslides, these zones partially coincide with the active fault traces in Figure 1. *Basili et al.* (1998) argue that the stripe described formed due to compaction of debris and lower slope deposits, because their observations suggested that the direction of movement was parallel to the maximum slope direction.

This paper tests whether the fresh stripe is produced by compaction or primary tectonic slip using theory that describes the geometry and kinematics of faulting and how this controls magnitudes of surface slip (*Faure Walker et al.*, 2009). Active faults in the Italian Apennines and central Greece show variability in their structure on a range of scales, including metre to kilometre scale corrugations and variations in the Holocene throw and slip direction along faults (*Roberts and Michetti*, 2004; *Roberts*, 2007; *Faure Walker et al.*, 2009; *Wilkinson et al.*, 2015). Faure Walker *et al.* (2009) demonstrated a quantitative relationship showing that strike, dip, Holocene throw and the slip vector of a fault are interrelated. Assuming that the principal strain rate is constant across a fault, if the strike becomes more oblique to the regional principal strain, for example around a bend in the fault plane, the throw rate of the fault will vary in order to preserve the principal strain rate (*Faure Walker et al.*, 2009). This theory is summarised in Figure 2 as a block diagram of a simple fault, more detail can be found in Faure Walker *et al.* (2009). This highlights the importance for knowing the local fault geometry if the total throw of a fault is used as a proxy for the activity of a fault. This relationship has the potential to differentiate between compaction and tectonic slip as the cause of the fresh stripe of rock along the bottom of the fault scarp. For the former, slip will show no relationship with the geometry and kinematics of bedrock faulting but may correlate with the hillside geomorphology, whilst for the latter we expect coseismic throw to increase where the strike and dip of the fault plane change relative to the slip-vector but should not show a correlation with the hillslope.

To study the above, high-spatial-resolution structural data has been collected, supported by TLS (Terrestrial Laser Scanning) of the geomorphology and slopes, along the Mt Le Scalette fault, situated on the Umbria-Marche regional border, near the town of Colfiorito. This fault (Figure 1) ruptured during at least one of the mainshocks of 1997 (Event 1 and/or Event 2), and is suggested by some to have ruptured at the surface (*Cello et al.,* 1998; *Vittori et al.,* 2000). We first review the structural setting of the earthquake before proceeding to an analysis of structural measurements on the bedrock faults and discussion of their link to the nodal plane dips for the earthquakes.

2. Geological background

The Italian Apennines are undergoing continental extension, located between the converging African and Eurasian plates (*Anderson and Jackson*, 1987). There is a narrow zone of convergence and thrusting along the Adriatic coast at the present day, whereas inland the thrusting ceased during the Pliocene (*Patacca et al.*, 1990). Present day extension began 2.5 Ma, evident by sediment and fossils infilling extensional basins (*Cavinato et al.*, 2002; *Roberts and Michetti*, 2004), defined by a series of normal faults striking north-west to south-east. The Italian peninsula has undergone long wavelength uplift since the early Pleistocene (*Girotti and Piccardi*, 1994; *Coltorti and Pieruccini*, 2000; *D'Agostino et al.*, 2001), and the distribution and strain-rates associated with the active faults correlates with this long wavelength topography (*Faure Walker et al.*, 2012; *Cowie et al.*, 2013).

Bedrock scarps in Mesozoic limestone are well-exposed in the Italian Apennines. It is hypothesised that these scarps are formed by tectonic exhumation and preserved since the end of the Last Glacial Maximum (LGM, 15±3 kyr) due to decreasing erosion rates (*Piccardi et al.*, 1999; *Galadini and Galli*, 2000; *Roberts and Michetti*, 2004, fig.7; *Tucker et al.*, 2011). This is confirmed by in situ ^{36}Cl cosmogenic isotope studies of the exhumation of the fault planes (*Palumbo et al.*, 2004, *Schlagenhauf et al.*, 2010, 2011).

In Umbria, the Mt Le Scalette and the Costa-San Martino faults form bedrock scarps in Jurassic and Cretaceous limestones, with Oligocene sediments exposed in the hanging walls. The stratigraphic throws across the Mt Le Scalette and Costa-San Martino faults are 550-600m (*Mirabella et al.*, 2005). The Mt Le Scalette fault borders the internally draining Colfiorito basin (*Calamita et al.*, 2000; *D'Agostino et al.*, 2009). The last known earthquake prior to 1997 in the area surrounding these faults was in 1279 A.D. (*Boschi*, 2000; *Guidoboni et al.*, 2007), but it is not possible to assign this earthquake conclusively to either fault due to sparse shaking records (*Guidoboni et al.*, 2007) and a lack of paleoseismic trenching on either fault. Instrumentally recorded earthquakes (1979 Norcia fault M_w=5.8; 1984 Gubbio fault M_w=5.6; 1997 Colfiorito earthquakes, $M_w \leq 6.0$; *Deschamps et al.*, 1984; *Westaway et al.*, 1989) all show normal faulting mechanisms, which is consistent with the present day tectonic extension (*Anderson and Jackson*, 1987; *Boncio et al.*, 2004; *D'Agostino et al.*, 2009). Here we concentrate on un-weathered stripes of exposed bedrock that are known to have been exhumed during the earthquake sequence, in an attempt to ascertain whether they have been exhumed by compaction or primary tectonic slip that can be linked to an earthquake at depth.

3. Methods

Detailed structural mapping was undertaken on the Mt Le Scalette fault (Figure 1) using a handheld Garmin GPS to record UTM coordinates of localities along the fault scarp, with a location accuracy of approximately ±5m. Structural data were measured on all exposed fault surfaces. Strike, dip and kinematic measurements were taken using a compass-clinometer along the fault scarp; these measurements have an accuracy of ±2°. Slip-vector azimuth measurements were taken from frictional wear striae on the bedrock scarps and from the geometry of large and small-scale corrugations. Previously Roberts (2007) has shown that where striae and corrugations are measured at the same locations on other faults in Italy and Greece, the same azimuth is recovered from each feature. Note that the fault slip-vector studied must be measured on the bedrock scarp itself and clearly be part of the structural geology of the fault. Thus, we measure the slip vector from frictional wear striae and corrugations associated with slickenslides on the bedrock. In contrast, Basili *et al.* (1998) measure displacements arising from soil sliding along planes coincident with the fault plane and they observe that the direction of displacements always seem to be parallel to the direction of maximum slope. We are aware that slip-vectors measured from deformed soils can converge into incised hangingwall gullies, suggesting overall down-slope movements (*Basili et al.*, 1998), but we specifically do not measure from such locations as they do not un-ambiguously record the tectonic slip vector, but rather record gravitationally-induced shallow mass wasting. At the base of the Mt Le Scalette scarp, a pale unweathered stripe is observed (Figure 3). The slip associated with this stripe was measured using a ruler. The upper edge of the stripe is defined where weathering increases over a few millimetres to centimetres to its top edge and the first occurrence of moss. The base is defined by the transition to soil in the hangingwall. We define the error in these measurements to be ±2 cm (see Fig. 2e and f for detail). The height of the stripe in the plane of the scarp (slip) was measured in the field and converted to vertical height (throw; using the measured dip). The structural data were analysed using Stereonet 8 (*Allmendinger et al.*, 2012). A structural map was constructed in the field, noting the location and extent of fans, gullies and other geomorphic features. Structural data from the bedrock scarp were added to this map following post-field analysis.

3.1. Terrestrial Laser Scanning

TLS data enabled us to interpret the surface geomorphology on a portion of the fault. The fault surface, footwall and hangingwall topography was captured as x-y-z coordinate point clouds using a Leica Scanstation C10 instrument. In addition to background intensity values, an onboard digital camera automatically acquired colour images that were used to RGB colour-code the point cloud data. Six separate scans were acquired in three different locations containing c. 30 million individual points in total. Scans were co-registered to a network of reflectors placed within the point cloud. The location of each reflector was surveyed using a differential GNSS and during post processing converted into the Universal Transverse Mercator (UTM) coordinate system (Zone 33 T). Individual scans were combined in Leica Geosystems HDS Cyclone™ software. To remove vegetation, the point cloud data was processed using a box-filter with three different box sizes depending on the density of point within the grid-area sampled. For areas of the point cloud where the number of points per m^2 was less than 2000, the lowest point in a 4 m^2 area was selected. Where the point cloud density was less than 10,000 points per m^2, the lowest point in every $1m^2$ was selected. For a greater density, the lowest point in every 0.5 m^2 was selected. Manual filtering was then used to remove any remnants of vegetation from the point cloud. A digital elevation model (DEM) was created by converting the filtered point cloud to a triangulated irregular network (TIN) and then to raster format by gridding the data at 1m resolution within a geographical information system (GIS). Two $10m^2$ areas were selected on the hangingwall and footwall slopes and aspect analysis were performed within the GIS. A topographic profile was extracted and interpreted from the raw TLS point cloud data.

4. Results

4.1 Structural Mapping

The structural map constructed (Figure 4) shows the fault scarp trace for a 600 m long section of the fault, with structural, kinematic and geomorphological data along the section. The constructed map shows that there is variability in the strike of the fault scarp and that corrugations/bends can be seen at many different scales. For example, a large-scale corrugation that is convex to the SW exists over a distance of ~350 m along strike between points B' and B on Figure 4 and is also evident on the strike versus distance graph in Figure 5a. Note this variability in the trace of the fault is a real corrugation (i.e. not just a change in map trace due to topography), confirmed by topographic contours (Figure 4) and the field measurements taken along the fault scarp (Figure 5a).

To test whether the slip-vector changes across the corrugation, the slip vector was measured at four locations across the corrugation between B' and B from frictional wear striae on the fault plane. The mean slip vector plunge and azimuth is 61^{o} towards

211°, with little variation between the 4 sites (< 13° variation defined by 202°, 206°, 212° and 215° for the azimuth values), despite the fact the strike changes by ~40° across the same corrugation. Thus, it appears that the mean slip-vector is in accord with the resolved shear strain from the larger-scale strain tensors on the fault plane (e.g. *Roberts*, 1996a, 1996b, 2007) and is unaffected by small-scale variations in fault geometry.

In order to test whether the slip-vector is related to the larger-scale strain tensors or local surface slopes as suggested by Basili *et al.* (1998), we have also measured the aspect (downslope direction) of the slopes around the fault scarp (Figure 4b and c). Our TLS results show that the downslope direction for the lower slope shows a strong peak at ~260°, whereas measurements of striae show that the mean slip-vector azimuth is 211° (Figure 4c). Thus, it is clear that the slip vector azimuth defined by faulting in the bedrock is not perpendicular to the slope defined by the TLS data and hence inconsistent with local gravity-driven compaction as the cause of the slip.

4.2 Interpretation of structural measurements

From the data presented in Figure 5, a systematic relationship between the strike, dip and coseismic throw is seen across the large-scale corrugation between B' and B (Figures 5a and b). When the strike is perpendicular to the sip vector azimuth (around 150m along the section in Figure 5), the dip and coseismic throw are at a minimum of 55-65° and 3-6cm respectively. Close to the lateral extremities of the corrugation (at 0-50m and 250-400m along the section in Figure 5), strikes are oblique to the tectonic slip vector azimuth of 211° and the measured dips are 60-80° and coseismic throw values are 7-12cm. Figure 5d confirms that the strike and dip are varying in tandem because a positive correlation is found across this corrugation. Again this suggests that the small-scale fault geometry and slip interact in response to the larger-scale strain tensors. These results and the systematic relationship observed in Figure 5 agrees with the theory presented in Faure Walker *et al.* (2009) and shown in Figure 2 in this paper.

Thus, we have a physical explanation for the structural variation we have measured that is rooted in an established theoretical framework. This is consistent with the hypothesis that surface slip evidenced by the fresh stripe is associated with tectonic slip on the bedrock scarp and inconsistent with the hypothesis of gravity-driven slip associated with compaction. The height of the stripe at the base of the Mt Le Scalette fault is assumed to be solely due to coseismic slip, as the free faces were observed for months following the mainshocks and no additional (post-seismic) slip was detected (*Vittori et al.*, 2000).

Our interpretation of tectonic slip across the scarp, rather than slip driven by compaction, suggests that we are able to extract a value for the cumulative tectonic slip and hence the tectonic slip-rate across the fault averaged within a time period given regional constraints on the age of the offset slopes. Using an age of 15 ±3 ka for the offset paleosurface and a value of 10.11 m for the offset derived from a scarp profile from our TLS dataset (see Figure 4a), we derive a throw-rate of 0.67 ± 0.13 $mmyr^{-1}$ since the demise of the LGM.

Similar bedrock scarps have been shown to be exhumed in the Holocene in central Italy using ^{36}Cl in situ cosmogenic exposure dating (e.g. *Palumbo et al.*, 2004; *Schlagenhauf et al.*, 2010, 2011; *Benedetti et al.*, 2013). This is consistent with tephrachronology and dated climate driven erosion rate changes that suggest the paleosurfaces date from the time of the demise of the last glacial maximum at 15 ±3 ka (see Roberts and Michetti (2004) for a review).

4.3. Reassessment of nodal plane dips

Cinti *et al.* (1999) suggested that the CMT dip projected from the hypocentre to the surface does not align with the observed fault scarps at surface (see *Cinti et al.*, 1999, fig.4). Also, Chiaraluce *et al.* (2005) proposed that there is a difference between the dips measured at the surface and at depth. These two observations have been used to suggest that the surface faults were not reactivated by primary tectonic slip during the earthquakes. However, as shown above in Section 4.1, up to ~25º variation in fault dip has been measured on the bedrock fault scarp and uncertainties exist for the hypocentral locations and nodal plane dips from the seismological data. Hence the ranges of surface and seismological dip data may overlap. Below we investigate whether we can reconcile the seismological data from depth with those measured at the surface to see if it is possible to exclude slip at depth propagating to the bedrock fault scarps at the surface.

Published hypocentres and dips for the three mainshocks of 1997 are shown in Figures 6 and 7. There is a large range in the depth and location for the same earthquake, as reported by different authors (*Amato et al.*, 1998; *Cello et al.*, 1998; *Boncio and Lavecchia*, 2000b; *Cattaneo et al.*, 2000; *Cocco et al.*, 2000; *Castello et al.*, 2006; *Chiarabba et al.*, 2009); this is due to different location methods, velocity models and station arrays being used. One set of hypocentres presented are preliminary locations

(*Cello et al.*, 1998) and hence are less reliable than later location studies. Another set of hypocentres are based on worldwide teleseismic arrivals (*ISC*, 2012) and are likely to have poorer location constraints. Certain locations are more precise than others, due to the use of a double difference location method (*Waldhauser and Ellsworth*, 2000) as used by *Chiaraluce et al.* (2003) and *Chiarabba et al.* (2009), or due to using a local network (*Cattaneo et al.*, 2000), or a 3D velocity model (*Chiarabba et al.*, 2009). Furthermore, for nodal plane dips, studies have concentrated on results computed by different moment tensor inversions (e.g. *Ekström et al.*, 1998; *Weston et al.*, 2011), fitting focal planes to arrival polarities (*Cattaneo et al.*, 2000), and from the aftershocks (*Chiaraluce et al.*, 2005). The range of dip values published in the literature is up to 23^{o} for a single event. Dip values obtained from aftershock alignment are reported in Chiaraluce *et al.* (2005). The aftershocks form a diffuse but planar alignment in the upper 7-8km of the crust. (see fig. 7, in *Chiaraluce et al.*, 2005). Hence the range in dips from aftershock alignment can be up to 30^{o}.

Some authors have suggested that the normal faults in the Apennines have a listric dip (*Boncio and Lavecchia*, 2000b; *Barchi and Mirabella*, 2009) based on seismic reflection profiles from Bally *et al.* (1986). This could reconcile the difference in dips between the surface measurements and nodal plane dips. However, studies of aftershock locations from the L'Aquila (*Valoroso et al.*, 2013), Colfiorito (*Chiaraluce et al.*, 2003) and Gualdo Tadino (*Ciaccio et al.*, 2005) earthquake sequences show that the aftershock alignments favour a planar fault at depth.

Taken together, we have compared hypocentral locations and nodal plane dips with measurements at the surface reported in Section 4.1. The results show that several of the hypocentral locations fall within the range of the down-dip projection of the surface trace of the fault from our structural measurements (i.e. within the black dashed lines delineating the range of data in Figure 6) and postulated dips overlap within error (Figure 7). Thus, the possibility that the earthquakes occurred on the down-dip projections of the surface faults cannot be excluded. We therefore reject the hypothesis that the earthquakes did not occur on the down-dip prolongation of the surface faults, and support the hypothesis that the surface faults were reactivated by primary tectonic slip during the earthquakes.

5. Discussion

A key question in seismic hazard is whether slip at depth in an earthquake propagates to the surface. If it does, the surface trace of the fault defines the exact location and geometry of a seismic source and hence can be used as an input for seismic hazard assessment (e.g. *Stirling et al.*, 2002; *Cheng et al.*, 2007; *Field et al.*, 2009, for other tectonically active regions). This informs modelling of slip distributions on the fault surface at depth for Italian and worldwide examples (e.g. *Stramondo et al.*, 1999 for the 1997 Colfiorito earthquake, Wald and Heton (1994) for the 1992 Landers earthquake, Ozawa *et al.* (2011) for the 2011 Tohoku earthquake) and hence expected ground shaking during an earthquake (e.g. *Barba and Basili*, 2000). Until now uncertainty has surrounded the question in the case of the 1997 Colfiorito earthquakes. Figure 1 shows both the "individual seismogenic sources" from DISS 3.2.0 (see Basili *et al.* (2008) for description of this database), and the surface traces of mapped faults that offset the surface geology from Mirabella *et al.* (2005). Clearly the simplified traces from DISS will yield simplified slip distributions and models of ground shaking if used in modelling seismological and geodetic data if the actual trace is that of Mirabella *et al.* (2005). Our findings herein suggest that the surface trace from Mirabella *et al.* (2005) does indeed mark the location where slip at depth propagated to the surface. We suggest that an improved understanding of the slip distribution and ground shaking would be achieved if the detailed surface fault trace were included in calculations.

Our results are not surprising. Surface faulting has been widely reported for a number of normal faulting earthquakes in the USA (e.g. DePolo *et al.* (1991) for a summary and Wallace *et al.* (1984) for the 1915 Pleasant Valley earthquake), Greece (e.g. *Jackson et al.*, 1982), Turkey (e.g. *Eyidogan and Jackson*, 1985),and Italy (1915 Fucino (*Oddone*, 1915; *Galadini et al.*, 1997) and 2009 L'Aquila (*Wilkinson et al.*, 2010; *Vittori et al.*, 2011)). It is widely believed that these are the primary surface expression of slip at depth propagating to the surface (*Jackson and White*, 1989; *Wells and Coppersmith*, 1994). Despite this, some examples from Italy of hypothesised primary surface slip have been rejected by some, usually with reference to the possible effects of ground-shaking and compaction producing surface rupture (e.g. Basili et al*.* (1998) and Barba and Basili (2000) for the 1997 Colfiorito earthquakes) or that the faults are sealed by Quaternary deposits (e.g. *Fubelli et al.*, 2009). If this were correct, it would suggest that there is something fundamentally different about normal faulting in Italy and this would be very significant if proven by observations. However, the findings of this paper suggest that for one of the best constrained examples from Italy, faulting at depth did indeed propagate to the surface, resembling the cases from tectonic settings listed above, and suggesting there is nothing fundamentally different about normal faulting in Italy.

The quantitative relationship presented in Faure Walker *et al.* (2009) demonstrates how the strike, dip and throw are interrelated along a fault trace while maintaining a constant principal strain rate. Specifically, the geometry-dependent throw-rate theory hypothesises that the average Holocene throw-rate increases across the fault where the deviation of the fault strike from the mean direction and the dip of the fault increases if the slip vector remains constant (*Faure Walker et al., 2009, 2015*). This relationship has been demonstrated for two faults in the central Apennines that display significant strike variations: the Parasano Fault (*Faure Walker et al., 2009*) and the Campo Felice Fault (*Wilkinson et al., 2015*). Faure Walker *et al.* (2009) noted the importance of strain rates controlling seismic hazard for a particular fault and hence care must be taken if the total throw is used as a proxy for the level of fault activity because of local geometry. The data presented in this paper is the first known example of a coseismic slip distribution broadly agreeing with the relationship and hence improves the reliability of the relationship.

We make three points that have wider significance:

1) This work highlights the difficulty of resolving subjective interpretations of surface deformation that do not involve structural geological analysis. We outline an approach where the question of primary surface faulting resulting from propagation of slip from depth can be assessed within a quantitative structural geology framework derived from theory that describes the geometric aspects of slip on non-planar, segmented faults in relation to strain tensors (*Faure Walker et al.*, 2009). We suggest that, where possible, (a) in the future, measurements of the strike, dip and slip-vector of bedrock faults associated with surface ruptures should be routinely measured before assessing surface ruptures as the result of primary surface faulting or ruptures resulting from shaking

and compaction, and (b) that other examples in the literature, especially in Italy (e.g. Basili *et al.* (1998) and Barba and Basili (2000)) should be revisited with this in mind.

2) We note that many examples exist in the literature (see Galli *et al.* (2008) for a review) where values for coseismic throw have been derived by palaeoseismologists for ancient earthquakes in the absence of discussion of the fault geometry and kinematics. This approach used herein suggests that values for coseismic throw measured from palaeoseismology need to be re-assessed taking into account whether the throw value comes from a location where the local fault geometry has produced anomalously large slip such as where the slip vector is not perpendicular to the fault trace, or a location that is more typical of the earthquake in question (see also *Faure Walker et al.*, 2015).

3) It is only possible to use observations of offset geomorphology of known age to infer rates of tectonic deformation if the surface offsets are produced by primary surface slip rather than gravity-driven compaction. Our observations suggest primary slip propagates to the surface, consistent with observations of ^{36}Cl in situ cosmogenic exposure dating on similar fault scarps in Italy (*Palumbo et al.*, 2004; *Schlagenhauf et al.*, 2010, 2011; *Benedetti et al.*, 2013). Suggestions to the contrary where surface deformation is hypothesised to result from gravity driven compaction during shaking invalidate the approach of tectonic geomorphology if correct; thus, such interpretations must be made with extreme caution. In this example we report that we reject the hypothesis that surface deformation is produced instead by gravity driven compaction during shaking. This allows us to derive a throw-rate averaged over many seismic cycles (15 ±3 ka) that would otherwise be dismissed. Our findings suggest that the approach

taken by tectonic geomorphologists is valid for this example, and also for other areas affected by normal faulting in Italy.

Overall, we suggest that with careful field structural geology, it is possible to gain insights into the normal faulting earthquakes that would be unavailable without the detailed structural mapping presented herein.

6. Conclusions

In this paper we present structural data from a surface bedrock scarp that displays a systematic relationship between the fault geometry and the coseismic throw. Hence we conclude that this fault scarp, and others that are exposed in the Apennines, are active and connected to the seismogenic structure at depth, agreeing with previously published work (e.g. Blumetti *et al.* (1993); Michetti *et al.* (2000); Vittori *et al.* (2011)). This is an important debate to resolve, as it has implications for utilising active fault traces for seismic hazard assessment in the region. This conclusion is not surprising when compared with other active normal fault systems around the world, such as the Basin and Range, Greece and Turkey. Our structural measurements from the Mt Le Scalette fault scarp highlight that the fault geometry and (coseismic) throw is systematically variable from metre to hundreds of metres scale. This is rarely appreciated or considered in other examples of faults in the Apennines, particularly in the field of paleoseismology. Coseismic slip is measured in paleoseismic trenches and can be used to infer the magnitude of past events (e.g. Galli *et al.* (2008)). However, without knowledge of the fault geometry at the trench location, the magnitude may be incorrectly estimated. Our conclusion also agrees with ^{36}Cl cosmogenic dating performed on similar bedrock scarps in Italy for two reasons. Firstly the exposure ages calculated from ^{36}Cl concentration indicate exposure throughout the Holocene, hence the faults are not inactive in the Holocene or sealed as suggested by some authors (*Fubelli et al.*, 2009). Secondly the exposure results obtained can only be explained by a coseismic slip history and not by a landslide or compaction history. Hence for any investigation of the active tectonics and paleo-earthquakes in the Italian Apennines we conclude that it is important to understand and analyse the local fault geometry so that results are valid.

Acknowledgments

This study was funded by the NERC Studentship NE/L501700/1 and the NERC grants (NE/E01545X/1 and NE/I024127/1). Comments from Laura Gregory (University of Leeds) helped to improve the manuscript.

References:

Allmendinger, R. W., N. Cardozo, and D. M. Fisher (2012), *Structural Geology Algorithms: Vectors and tensors*, 1st ed., Cambridge University Press.

Amato, A., R. Azzara, C. Chiarabba, G. B. Cimini, M. Cocco, M. Di Bona, L. Margheriti, S. Mazza, F. Mele, G. Selvaggi, A. Basili, E. Boschi, F. Courboulex, A. Deschamps, S. Gaffet, G. Bittarelli, L. Chiaraluce, D. Piccinini, and M. Ripepe (1998), The 1997 Umbria-Marche, Italy, earthquake sequence: A first look at the main shocks and aftershocks, *Geophys. Res. Lett.*, *25*(15), 2861–2864.

Anderson, H., and J. A. Jackson (1987), Active tectonics of the Adriatic Region, *Geophys. J. Int.*, *91*, 937–983.

Anzidei, M., P. Baldi, A. Galvani, A. Pesci, I. Hunstad, and E. Boschi (1999), Coseismic displacement of the 27th September 1997 Umbria-Marche (Italy) earthquakes detected by GPS: campaigns and data, *Ann. di Geofis.*, *42*(4), 597–607.

Bally, A. W., L. Burbi, C. Cooper, and R. Ghelardoni (1986), Balanced sections and seismic reflection profiles across the Central Apennines, *Mem. Soc. Geol. It*, *35*(1), 257–310.

Barba, S., and R. Basili (2000), Analysis of seismological and geological observations for moderate-size earthquakes: The Colfiorito Fault System (Central Apennines, Italy), *Geophys. J. Int.*, *141*(1), 241–252, doi:10.1046/j.1365-246X.2000.00080.x.

Barchi, M. R., and F. Mirabella (2009), The 1997–98 Umbria–Marche earthquake sequence: “Geological” vs. “seismological” faults, *Tectonophysics*, *476*(1-2), 170–179, doi:10.1016/j.tecto.2008.09.013.

Basili, R., V. Bosi, F. Galadini, P. Galli, M. Meghraoui, P. Messina, M. Moro, and A. Sposato (1998), The Colfiorito Earthquake Sequence of September–October 1997: Surface Breaks and Seismotectonic Implications for the Central Apennines (Italy), *J. Earthq. Eng.*, *2*(January 2015), 291–302, doi:10.1080/13632469809350323.

Basili, R., G. Valensise, P. Vannoli, P. Burrato, U. Fracassi, S. Mariano, M. M. Tiberti, and E. Boschi (2008), The Database of Individual Seismogenic Sources (DISS), version 3: Summarizing 20 years of research on Italy’s earthquake geology, *Tectonophysics*, *453*(1-4), 20–43, doi:10.1016/j.tecto.2007.04.014.

Benedetti, L., I. Manighetti, Y. Gaudemer, R. Finkel, J. Malavieille, K. Pou, M. Arnold, G. Aumaître, D. Bourlès, and K. Keddadouche (2013), Earthquake synchrony and clustering on Fucino faults (Central Italy) as revealed from in situ 36 Cl exposure dating, *J. Geophys. Res. Solid Earth*, *118*(9), 4948–4974, doi:10.1002/jgrb.50299.

Blumetti, A. M., F. Dramis, and A. M. Michetti (1993), Fault-generated mountain fronts in the central apennines (Central Italy): Geomorphological features and seismotectonic implications, *Earth Surf. Process. Landforms*, *18*(3), 203–223, doi:10.1002/esp.3290180304.

Boncio, P., and G. Lavecchia (2000a), A geological model for the Colfiorito earthquakes (September-October 1997, central Italy), *J. Seismol.*, *4*, 345–356.

Boncio, P., and G. Lavecchia (2000b), A structural model for active extension in Central Italy, *J. Geodyn.*, *29*, 233–244.

Boncio, P., G. Lavecchia, and B. Pace (2004), Defining a model of 3D seismogenic sources for Seismic Hazard Assessment applications: The case of central Apennines (Italy), *J. Seismol.*, *8*(3), 407–425, doi:10.1023/B:JOSE.0000038449.78801.05.

Boschi, E. (2000), Earthquake of 30 April 1279, Umbria-Marche Apennines, *Ann. di Geofis.*, *43*.

Calamita, F., M. Coltorti, D. Piccinini, P. P. Pierantoni, A. Pizzi, M. Ripepe, V. Scisciani, and E. Turco (2000), Quaternary faults and seismicity in the Umbro-Marchean Apennines (Central Italy): Evidence from the 1997 Colfiorito earthquake, *J. Geodyn.*, *29*(3-5), 245–264, doi:10.1016/S0264-3707(99)00054-X.

Castello, B., G. Selvaggi, C. Chiarabba, and A. Amato (2006), CSI Catalogo della sismicità italiana 1981-2002, *INGV-CNT Roma*. Available from: http://csi.rm.ingv.it/versione_inglese/index_eng.htm

Cattaneo, M., P. Augliera, G. De Luca, A. Gorini, A. Govoni, S. Marcucci, A. Michelini, G. Monachesi, D. Spallarossa, and L. Trojani (2000), The 1997 Umbria-Marche (Italy) earthquake sequence: Analysis of the data recorded by the local and temporary networks, *J. Seismol.*, *4*, 401–414.

Cavinato, G. P., C. Carusi, M. Dall'asta, E. Miccadei, and T. Piacentini (2002), Sedimentary and tectonic evolution of Plio-Pleistocene alluvial and lacustrine deposits of Fucino Basin (central Italy), *Sediment. Geol.*, *148*, 29–59, doi:10.1016/S0037-0738(01)00209-3.

Cello, G., G. Deiana, P. Mangano, S. Mazzoli, E. Tondi, L. Ferreli, L. Maschio, A. M. Michetti, L. Serva, and E. Vittori (1998), Evidence for surface faulting during the September 26, 1997, Colfiorito (central Italy) earthquakes, *J. Earthq. Eng.*, *2*(2), 303–324, doi:10.1080/13632469809350324.

Cello, G., G. Deiana, L. Ferelli, L. Marchegiani, L. Maschio, S. Mazzoli, A. M. Michetti, L. Serva, E. Tondi, and T. Vittori (2000), Geological constraints for earthquake faulting studies in the Colfiorito area (central Italy), *J. Seismol.*, *4*, 357–364.

Cheng, C.-T., S.-J. Chiou, C.-T. Lee, and Y.-B. Tsai (2007), Study on Probabilistic Seismic Hazard Maps of Taiwan after Chi Chi Earthquake, *J. Geoengin.*, *2*(1), 19–28, doi:10.6310/jog.2007.2(1).3.

Chiarabba, C., D. Piccinini, and P. De Gori (2009), Velocity and attenuation tomography of the Umbria Marche 1997 fault system: Evidence of a fluid-governed seismic sequence, *Tectonophysics*, *476*(1-2), 73–84, doi:10.1016/j.tecto.2009.04.004.

Chiaraluce, L., W. L. Ellsworth, C. Chiarabba, and M. Cocco (2003), Imaging the complexity of an active normal fault system: The 1997 Colfiorito (central Italy) case study, *J. Geophys. Res.*, *108*(B6), 2294, doi:10.1029/2002JB002166.

Chiaraluce, L., M. R. Barchi, C. Collettini, F. Mirabella, and S. Pucci (2005), Connecting seismically active normal faults with Quaternary geological structures in a complex extensional environment: The Colfiorito 1997 case history (northern Apennines, Italy), *Tectonics*, *24*(1), doi:10.1029/2004TC001627.

Ciaccio, M. G., M. R. Barchi, C. Chiarabba, F. Mirabella, and E. Stucchi (2005), Seismological, geological and geophysical constraints for the Gualdo Tadino fault, Umbria–Marche Apennines (central Italy), *Tectonophysics*, *406*(3-4), 233–247, doi:10.1016/j.tecto.2005.05.027.

Cinti, F. R., L. Cucci, F. Marta, and P. Montone (1999), The 1997 Umbria-Marche (Italy) earthquake sequence: relationship between ground deformation and seismogenic structure., *Geophys. Res. Lett.*, *26*(7), 895–898.

Cinti, F. R., L. Cucci, F. Marra, and P. Montone (2000), The 1997 Umbria-Marche earthquakes (Italy): Relation between the surface tectonic breaks and the area of deformation, *J. Seismol.*, *4*(4), 333–343, doi:10.1023/A:1026575219394.

Cocco, M., C. Nostro, and G. Ekström (2000), Static stress changes and fault interaction during the 1997 Umbria-Marche earthquake sequence, *J. Seismol.*, *4*, 501–516.

Coltorti, M., and P. Pieruccini (2000), A late Lower Pliocene planation surface across the Italian Peninsula: A key tool in neotectonic studies, *J. Geodyn.*, *29*(3-5), 323–328, doi:10.1016/S0264-3707(99)00049-6.

Cowie, P. A., C. H. Scholz, G. P. Roberts, J. P. Faure Walker, and P. Steer (2013), Viscous roots of active seismogenic faults revealed by geologic slip rate variations, *Nat. Geosci.*, *6.12*(November), 1036–1040, doi:10.1038/ngeo1991.

D'Agostino, N., J. A. Jackson, F. Dramis, and R. Funiciello (2001), Interactions between mantle upwelling, drainage evolution and active normal faulting: an example from the central Apennines (Italy), *Geophys. J. Int.*, *147*(2), 475–497, doi:10.1046/j.1365-246X.2001.00539.x.

D’Agostino, N., S. Mantenuto, E. D’Anastasio, A. Avallone, M. R. Barchi, C. Collettini, F. Radicioni, A. Stoppini, and G. Fastellini (2009), Contemporary crustal extension in the Umbria–Marche Apennines from regional CGPS networks and comparison between geodetic and seismic deformation, *Tectonophysics*, *476*, 3–12, doi:10.1016/j.tecto.2008.09.033.

DePolo, C. M., D. G. Clark, D. B. Slemmons, and A. R. Ramelli (1991), Historical surface faulting in the Basin and Range province, western North America: implications for fault segmentation, *J. Struct. Geol.*, *13*(2), 123–136, doi:10.1016/0191-8141(91)90061-M.

Deschamps, A., G. Iannacoone, and R. Scarpa (1984), The Umbrian earthquake (Italy) of 19 September 1979, *Ann. Geophys.*, *2*(1), 29–36.

Deschamps, A., F. Courboulex, S. Gaffet, A. Lomax, J. Virieux, A. Amato, A. Azzara, C. Chiarabba, G. B. Cimini, M. Cocco, M. Di Bona, L. Margheriti, F. Mele, L. Chiaraluce, D. Piccinini, and M. Ripepe (2000), Spatio-temporal distribution of seismic activity during the Umbria-Marche crisis, 1997, *J. Seismol.*, 377–386.

Dziewonski, A. M., G. Ekström, and N. N. Maternovskaya (2003), Centroid-moment tensor solutions for July–September 1997, *Phys. Earth Planet. Inter.*, *136*(3-4), 119–131, doi:10.1016/S0031-9201(03)00031-1.

Ekström, G., A. Morelli, E. Boschi, and A. M. Dziewonski (1998), Moment tensor analysis of the central Italy earthquake sequence of September-October 1997, *Geophys. Res. Lett.*, *25*(11), 1971–1974.

Eyidogan, H., and J. A. Jackson (1985), A seismological study of normal faulting in the Demirci, Alasehir and Gediz earthquakes of 1969-70 in western Turkey:

implications for the nature and geometry of deformation in the continental crust, *Geophys. J. Int.*, *81*(3), 569–607, doi:10.1111/j.1365-246X.1985.tb06423.x.

Faure Walker, J., G. P. Roberts, and K. J. W. Mccaffrey (2015), Long-term strain rates as a tool for understanding the mechanics of continental extension and the importance of local 3D fault geometry for local throw-rates across faults, *INQUA Focus Gr. Paleoseismology Act. Tectonics*.

Faure Walker, J. P., G. P. Roberts, P. A. Cowie, I. D. Papanikolaou, P. R. Sammonds, A. M. Michetti, and R. J. Phillips (2009), Horizontal strain-rates and throw-rates across breached relay zones, central Italy: Implications for the preservation of throw deficits at points of normal fault linkage, *J. Struct. Geol.*, *31*(10), 1145–1160, doi:10.1016/j.jsg.2009.06.011.

Faure Walker, J. P., G. P. Roberts, P. R. Sammonds, and P. A. Cowie (2010), Comparison of earthquake strains over 10 2 and 10 4 year timescales: Insights into variability in the seismic cycle in the central Apennines, Italy, *J. Geophys. Res.*, *115*(B10), B10418, doi:10.1029/2009JB006462.

Faure Walker, J. P., G. P. Roberts, P. A. Cowie, I. D. Papanikolaou, A. M. Michetti, P. R. Sammonds, M. Wilkinson, K. J. W. McCaffrey, and R. J. Phillips (2012), Relationship between topography, rates of extension and mantle dynamics in the actively-extending Italian Apennines, *Earth Planet. Sci. Lett.*, *325-326*, 76–84, doi:10.1016/j.epsl.2012.01.028.

Field, E. H., T. E. Dawson, K. R. Felzer, A. D. Frankel, V. Gupta, T. H. Jordan, T. Parsons, M. D. Petersen, R. S. Stein, R. J. Weldon, and C. J. Wills (2009), Uniform California earthquake rupture forecast, version 2 (UCERF 2), *Bull. Seismol. Soc. Am.*, *99*(4), 2053–2107, doi:10.1785/0120080049.

Fubelli, G., S. Gori, E. Falcucci, F. Galadini, and P. Messina (2009), Geomorphic signatures of recent normal fault activity versus geological evidence of inactivity: Case studies from the central Apennines (Italy), *Tectonophysics*, *476*(1-2), 252–268, doi:10.1016/j.tecto.2008.10.026.

Galadini, F., and P. Galli (2000), Active Tectonics in the Central Apennines (Italy)– Input Data for Seismic Hazard Assessment, *Nat. Hazards*, *22*, 225–270.

Galadini, F., P. Galli, and C. Giraudi (1997), Geological investigations of Italian earthquakes: new paleoseismological data from the Fucino Plain (central Italy), *J. Geodyn.*, *24*, 87–103.

Galli, P., F. Galadini, and D. Pantosti (2008), Twenty years of paleoseismology in Italy, *Earth-Science Rev.*, *88*(1-2), 89–117, doi:10.1016/j.earscirev.2008.01.001.

Girotti, O., and L. Piccardi (1994), Linee di riva del Pleistocene inferiore sul versante sinistro della Media Valle del fiume Tevere, *Quat.*, *7*, 525–536.

Guidoboni, E., G. Ferrari, D. Mariotti, A. Comastri, G. Tarabusi, and G. Valensise (2007), CFTI4Med, Catalogue of Strong Earthquakes in Italy (461B.C.-1997) and Mediterranean Area (760B.C.-1500), *INGV-SGA*. Available from: http://storing.ingv.it/cfti4med/

ISC (2012), International Seismological Centre, On-line Bulletin, *Internatl. Seis. Cent., Thatcham, United Kingdom*, http://www.isc.ac.uk. Available from: http://www.isc.ac.uk

Jackson, J. A., and N. J. White (1989), Normal faulting in the upper continental crust: observations from regions of active extension, *J. Struct. Geol.*, *11*(1-2), 15–36, doi:10.1016/0191-8141(89)90033-3.

Jackson, J. A., J. Gagnepain, G. Houseman, G. C. P. King, P. Papadimitriou, C. Soufleris, and J. Virieux (1982), Seismicity, normal faulting, and the geomorphological development of the Gulf of Corinth (Greece): the Corinth earthquakes of February and March 1981, *Earth Planet. Sci. Lett.*, *57*(2), 377–397, doi:10.1016/0012-821X(82)90158-3.

Michetti, A. M., L. Ferreli, E. Esposito, S. Porfido, A. M. Blumetti, E. Vittori, L. Serva, and G. P. Roberts (2000), Ground effects during the 9 September 1998, Mw=5.6, Lauria earthquake and the seismic potential of the “aseismic” Pollino region in Southern Italy, *Seismol. Res. Lett.*, *71*(1).

Mirabella, F., V. Boccali, and M. R. Barchi (2005), Segmentation and interaction of normal faults within the Colfiorito fault system (central Italy), *Geol. Soc. London, Spec. Publ.*, *243*(1), 25–36, doi:10.1144/GSL.SP.2005.243.01.04.

Oddone, E. (1915), Gli elementi fisici del grande terremoto marsicano-fucense del 13 gennaio 1915, *Boll. della Soc. Sismol. Ital.*, *19*, 71–291.

Ozawa, S., T. Nishimura, H. Suito, T. Kobayashi, M. Tobita, and T. Imakiire (2011), Coseismic and postseismic slip of the 2011 magnitude-9 Tohoku-Oki earthquake., *Nature*, *475*(7356), 373–376, doi:10.1038/nature10227.

Palumbo, L., L. Benedetti, D. Bourlès, A. Cinque, and R. Finkel (2004), Slip history of the Magnola fault (Apennines, Central Italy) from 36Cl surface exposure dating: evidence for strong earthquakes over the Holocene, *Earth Planet. Sci. Lett.*, *225*(1-2), 163–176, doi:10.1016/j.epsl.2004.06.012.

Patacca, E., R. Sartori, and P. Scandone (1990), Tyrrhenian basin and Apenninc arcs: kinematic relations since Late Tortonian times., *Mem. Soc. Geol. It*, *45*, 425–451.

Piccardi, L., Y. Gaudemer, P. Tapponnier, and M. Boccaletti (1999), Active oblique extension in the central Apennines (Italy): evidence from the Fucino region, *Geophys. J. Int.*, *139*(2), 499–530, doi:10.1046/j.1365-246x.1999.00955.x.

Ripepe, M., D. Piccinini, and L. Chiaraluce (2000), Foreshock sequence of The September 26th , 1997 Umbria-Marche earthquakes, *J. Seismol.*, 387–399.

Roberts, G. P. (1996a), Noncharacteristic normal faulting surface ruptures from the Gulf of Corinth, Greece, *J. Geophys. Res.*, *101*, 25255–25267.

Roberts, G. P. (1996b), Variation in fault-slip directions along active and segmented normal fault systems, *J. Struct. Geol.*, *18*(6), 835–845, doi:10.1016/S0191-8141(96)80016-2.

Roberts, G. P. (2007), Fault orientation variations along the strike of active normal fault systems in Italy and Greece: Implications for predicting the orientations of subseismic-resolution faults in hydrocarbon reservoirs, *Am. Assoc. Pet. Geol. Bull.*, *91*(1), 1–20, doi:10.1306/08300605146.

Roberts, G. P., and A. M. Michetti (2004), Spatial and temporal variations in growth rates along active normal fault systems: an example from The Lazio–Abruzzo Apennines, central Italy, *J. Struct. Geol.*, *26*(2), 339–376, doi:10.1016/S0191-8141(03)00103-2.

Roberts, G. P., P. A. Cowie, I. D. Papanikolaou, and A. M. Michetti (2004), Fault scaling relationships, deformation rates and seismic hazards: an example from the Lazio–Abruzzo Apennines, central Italy, *J. Struct. Geol.*, *26*(2), 377–398, doi:10.1016/S0191-8141(03)00104-4.

Schlagenhauf, A., Y. Gaudemer, L. Benedetti, I. Manighetti, L. Palumbo, I. Schimmelpfennig, R. Finkel, and K. Pou (2010), Using in situ Chlorine-36 cosmonuclide to recover past earthquake histories on limestone normal fault scarps: A reappraisal of methodology and interpretations, *Geophys. J. Int.*, *182*(1), 36–72, doi:10.1111/j.1365-246X.2010.04622.x.

Schlagenhauf, A., I. Manighetti, L. Benedetti, Y. Gaudemer, R. Finkel, J. Malavieille, and K. Pou (2011), Earthquake supercycles in Central Italy, inferred from 36Cl exposure dating, *Earth Planet. Sci. Lett.*, *307*(3-4), 487–500, doi:10.1016/j.epsl.2011.05.022.

Stirling, M. W., G. H. McVerry, and K. R. Berryman (2002), A new seismic hazard model for New Zealand, *Bull. Seismol. Soc. Am.*, *92*(5), 1878–1903, doi:10.1785/0120010156.

Stramondo, S., M. Tesauro, P. Briole, E. Sansosti, S. Salvi, R. Lanari, M. Anzidei, P. Baldi, G. Fornaro, A. Avallone, M. F. Buongiorno, G. Franceschetti, and E. Boschi (1999), The September 26 , 1997 Colfiorito , Italy , earthquakes: modeled coseismic surface displacement from SAR interferometry and GPS, *Geophys. Res. Lett.*, *26*(7), 883–886.

Tucker, G. E., S. W. McCoy, A. C. Whittaker, G. P. Roberts, S. T. Lancaster, and R. J. Phillips (2011), Geomorphic significance of postglacial bedrock scarps on normal-fault footwalls, *J. Geophys. Res. Earth Surf.*, *116*(F1), n/a–n/a, doi:10.1029/2010JF001861.

Valoroso, L., L. Chiaraluce, D. Piccinini, R. Di Stefano, D. Schaff, and F. Waldhauser (2013), Radiography of a normal fault system by 64,000 high-precision earthquake locations: The 2009 L'Aquila (central Italy) case study, *J. Geophys. Res. Solid Earth*, *118*(3), 1156–1176, doi:10.1002/jgrb.50130.

Vittori, E., G. Deiana, E. Esposito, L. Ferreli, L. Marchegiani, G. Mastrolorenzo, A. M. Michetti, S. Porfido, L. Serva, A. L. Simonelli, and E. Tondi (2000), Ground effects and surface faulting in the September-October 1997 Umbria-Marche (central Italy) seismic sequence, *J. Geodyn.*, *29*, 535–564.

Vittori, E., P. Di Manna, A. M. Blumetti, V. Comerci, L. Guerrieri, E. Esposito, A. M. Michetti, S. Porfido, L. Piccardi, G. P. Roberts, A. Berlusconi, F. Livio, G. Sileo, M. Wilkinson, K. J. W. McCaffrey, R. J. Phillips, and P. A. Cowie (2011), Surface Faulting of the 6 April 2009 Mw 6.3 L'Aquila Earthquake in Central Italy, *Bull. Seismol. Soc. Am.*, *101*(4), 1507–1530, doi:10.1785/0120100140.

Wald, D. J., and T. H. Heton (1994), Spatial and temporal distribution of slip for the 1992 Landers, California, earthquake, *Bull. Seismol. Soc. Am.*, *84*(3), 668–691.

Waldhauser, F., and W. L. Ellsworth (2000), A Double-Difference earthquake location algorithm: Method and application to the Northern Hayward Fault, California, *Bull. Seismol. Soc. Am.*, *90*(December), 1353–1368.

Wallace, R. E., M. G. Bonilla, and H. A. Villalobos (1984), Faulting Related to the 1915 Earthquakes in Pleasant Valley, Nevada, *USGSPO*, *1274-A*.

Wells, D. L., and K. J. Coppersmith (1994), New Empirical Relationships among Magnitude, Rupture Length, Rupture Width, Rupture Area, and Surface Displacement, *Bull. Seismol. Soc. Am.*, *84*(4), 974–1002.

Westaway, R., R. L. Gawthorpe, and M. Tozzi (1989), Seismological and field observations of the 1984 Lazio-Abruzzo earthquakes: implications for the active tectonics of Italy, *Geophys. J. Int.*, *98*(3), 489–514, doi:10.1111/j.1365-246X.1989.tb02285.x.

Weston, J., A. M. G. Ferreira, and G. J. Funning (2011), Global compilation of interferometric synthetic aperture radar earthquake source models: 1.

Comparisons with seismic catalogs, *J. Geophys. Res.*, *116*(B8), B08408, doi:10.1029/2010JB008131.

Wilkinson, M., K. J. W. McCaffrey, G. P. Roberts, P. A. Cowie, R. J. Phillips, A. M. Michetti, E. Vittori, L. Guerrieri, A. M. Blumetti, A. Bubeck, A. Yates, and G. Sileo (2010), Partitioned postseismic deformation associated with the 2009 Mw 6.3 L'Aquila earthquake surface rupture measured using a terrestrial laser scanner, *Geophys. Res. Lett.*, *37*(10), 1–7, doi:10.1029/2010GL043099.

Wilkinson, M., G. P. Roberts, K. J. W. McCaffrey, P. A. Cowie, J. P. Faure Walker, I. D. Papanikolaou, R. J. Phillips, A. M. Michetti, E. Vittori, L. Gregory, L. Wedmore, and Z. K. Watson (2015), Slip distributions on active normal faults measured from LiDAR and field mapping of geomorphic offsets: an example from L'Aquila, Italy, and implications for modelling seismic moment release, *Geomorphology*, *237*, 130–141, doi:10.1016/j.geomorph.2014.04.026.

Zollo, A., S. Marcucci, G. Milana, and P. Capuano (1999), The 1997 Umbria-Marche (central Italy) earthquake sequence: Insights on the mainshock ruptures from near source strong motion records., *Geophys. Res. Lett.*, *26*, 3165–3168.

Figure Captions

Figure 1: Summary map of the studied region. Map shows the location of towns and the active normal faults (red lines), ATR=Atri, CAS=Casci, CSM= Costa-San Martino, GUB=Gubbio, GUT= Gualdo Tadino, GU2=Gubbio 2, LAG= Laga, LEO=Leonessa, MAL= Mt. Alvagnano, MAR= Martana, MLS= Mt. Le Scalette, MSV=Mt. San Vicino, MVT= Mt. Vettore, NOR= Norcia, TER= Terni, UMV= Umbra Valley. Lower hemisphere focal mechanisms for the three mainshocks of the 1997 Umbria-Marche seismic sequence are shown, black mechanisms are from the CMT

catalogue (*Dziewonski et al.*, 2003), blue mechanism is from *Cattaneo et al.*, 2000c. Purple rectangle shows the extent of Figure 4. Inset shows the location of the main map as a blue box within Italy.

Figure 2- Block diagrams illustrating the relationship between the strike, dip and throw of a normal fault. (a) Simplified fault where the central section exhibits a bend. The slip vector azimuth remains constant across the fault (black arrows). Adapted from Figure 3, Faure Walker et al (2015). (b) The surface trace of the fault, with the central bend labelled. Adapted from fig. 3, Faure Walker et al (2015). (c) Graphs showing how the throw rate is expected to vary in the central section relative to the main fault as the strike or dip are varied independently. The principal strain rate is assumed to be constant across the fault trace. Adapted from Figure 6c and 7c, Faure Walker et al (2009). It is shown as the orientation of the central section becomes more oblique to the slip vector or the dip increases, the relative throw rate is expected to increase for a constant principal strain rate.

Figure 3: View of a section of the Mt Le Scalette fault scarp, close to the centre of the large scale corrugation mapped in Figure 3. a.) Views along the bedrock scarp, looking to the north-west. b.) view onto the bedrock scarp. White dashed box shows the extent of c.)close up of the base of the bedrock scarp, note that there is a fresh stripe at the base, which is also marked by the lack of moss growth (especially to the left hand side of the photograph. The unweathered stripe at the base of the scarp marked in a dashed red line.

Figure 4: Structural and geomorphic map of a well-exposed section close to the centre of

the Mt Le Scalette fault. Strike and dip data are grouped together over 20m sections, the mean strike and dip are reported on the map and the corresponding stereonets are shown. Kinematic indicators were found at four localities along the section, the mean slip-vector plunge and azimuth are reported on the map and the corresponding stereonets shown. The mean slip vector is 61 –> 211. The topographic profile created from the TLS data gives the Holocene throw of the fault and the Holocene throw rate is calculated from this. B – B' indicates the orientation of the data plotted in Figure 5. The white dashed box around the profile line A-A' indicates the extent of b.) hillshade DEM with 2m contours from a TLS survey. The fault scarp and upper slope boundary are marked. The mean slip vector and orientation of the upper and lower slope are marked. c.) frequency plot of the aspect of the lower and upper slopes from the TLS data. The mean trend of the slip vector measured from frictional wear striae on the fault plane does not align with the direction of maximum slope.

Figure 5: All structural data collected and plotted against distance along the fault, indicated by B – B' in Figure 3. a.) strike against distance, uncertainties are smaller than the symbols, the black line is perpendicular to the mean trend, the grey shaded region is the 95% confidence interval of the trend (calculated from Stereonet). b.) dip against distance, uncertainties are smaller than the symbols, the black line is the mean plunge, the grey shaded region is the 95% confidence interval of the trend. c.) vertical height of the unweathered stripe against distance. d.) strike against dip, data points are mean strike and dip values for 20m sections of the fault (see Figure 4) with 95% confidence interval plotted as the error. A

systematic relationship can be seen between the strike, dip and height of the stripe from these diagrams.

Figure 6: Map and cross sections of different published locations for the three mainshocks of the 1997 seismic sequence. a.) map view of the Colfiorito region affected by the 1997 seismic sequence. The traces of active normal faults are marked in red. Coloured circles refer to different published locations; (1) *Cello et al.*, 1998, (2) INGV, *Castello et al.*, 2006, (3) *Boncio and Lavecchia*, 2000a, (4) *ISC*, 2012, (5) *Amato et al.*, 1998, (6) *Cocco et al.*, 2000, (7) *Cattaneo et al.*, 2000, (8) *Chiarabba et al.*, 2009. Stereonets show the mean strike and dip for the two faults, MLS=Mt Le Scalette fault, CSM= Costa-San Martino fault. b.) cross-section of Event 1, c.) cross-section of Event 2, d.) cross-section of Event3. Cross-sections show the reported errors for each location, where published and the different reported dips for each earthquake. The red line indicates mean measured dip of each fault, projected to depth, with the 95% and 99% confidence intervals and full range of measured dips. This demonstrates that when the range of locations and dips are taken into account, there is overlap between the projected dip from the surface and the locations of earthquakes at depth and hence the surface fault scarps should be considered as active.

Figure 7: Comparing published dips of the three mainshocks to the dip of the surface fault scarps (from field measurements). Dips at depth are calculated by different methods and published by (1) *Ekström et al.*, 1998, (2) *Weston et al.*, 2011, (3) *Cattaneo et al.*, 2000, (4) *Zollo et al.*, 1999, (5) *Chiaraluce et al.*, 2005. Field

measurements of the dip were measured from bedrock fault scarp by the authors along the Mt Le Scalette and Costa-San Martino faults. For each event, there is an overlap between the dip at depth (from the literature) and the dip of the surface scarp. Hence, it cannot be argued that the surface scarps are inactive due to a mismatch between dip at depth and dip at the surface.

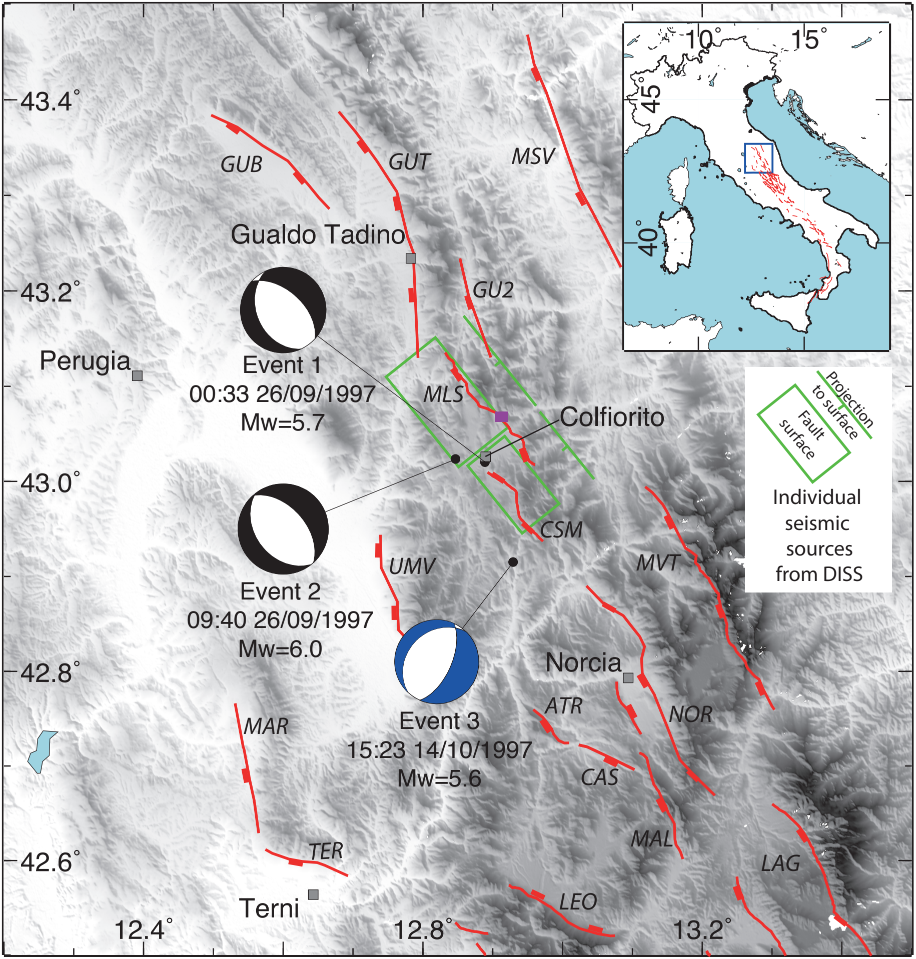

10°
15°
45°
40°
43.4°
43.2°
43.0°
42.8°
42.6°
12.4°
12.8°
13.2°
GUB
GUT
MSV
Gualdo Tadino
GU2
Perugia
Event 1
00:33 26/09/1997
Mw=5.7
MLS
Colfiorito
Projection to surface
Fault surface
Individual seismic sources from DISS
Event 2
09:40 26/09/1997
Mw=6.0
CSM
UMV
MVT
Norcia
Event 3
15:23 14/10/1997
Mw=5.6
ATR
NOR
MAR
CAS
MAL
LAG
TER
LEO
Terni

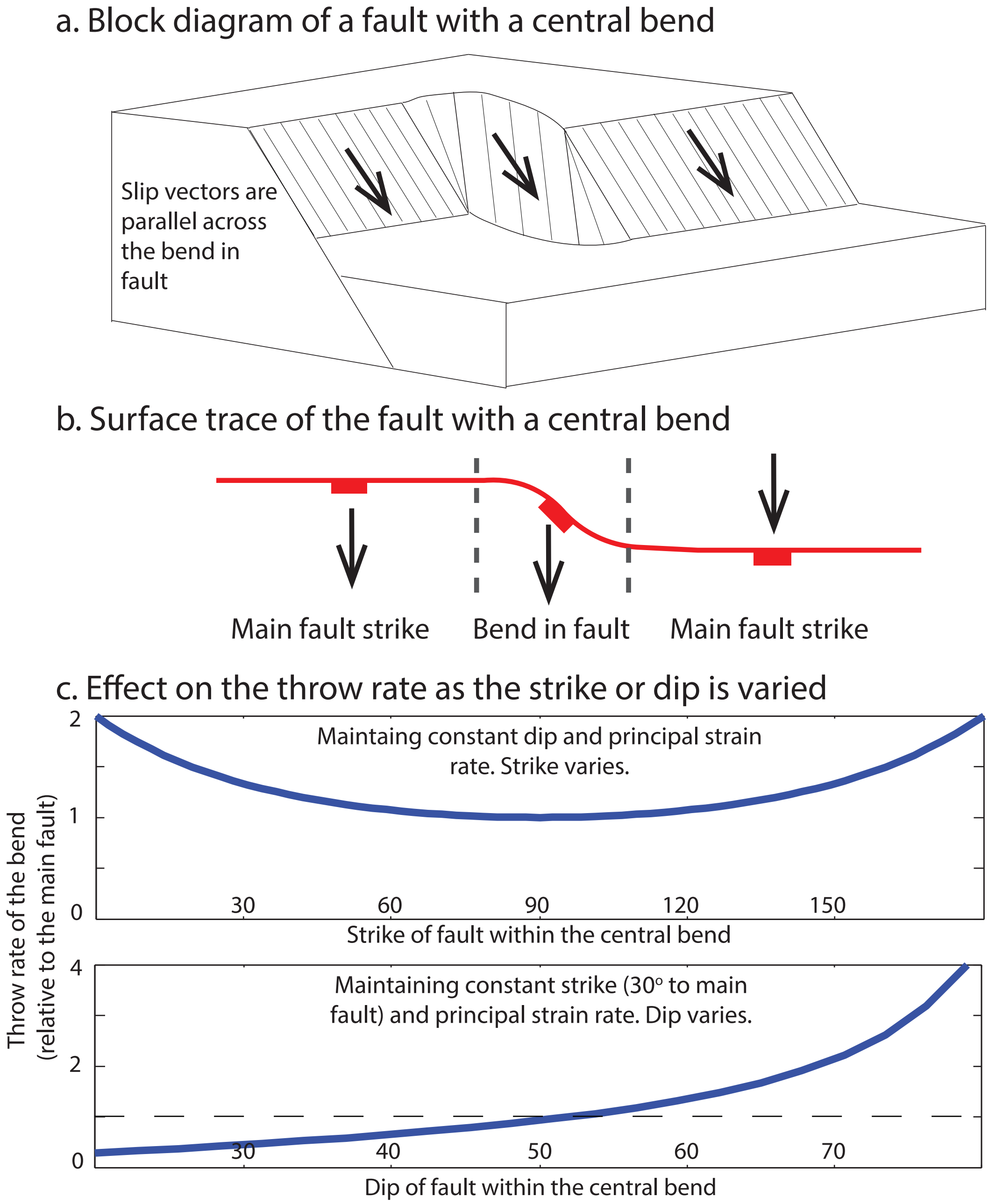
a. Block diagram of a fault with a central bend
Slip vectors are parallel across the bend in fault
b. Surface trace of the fault with a central bend
Main fault strike
Bend in fault
Main fault strike
c. Effect on the throw rate as the strike or dip is varied
Maintaing constant dip and principal strain rate. Strike varies.
Strike of fault within the central bend
Maintaining constant strike (30º to main fault) and principal strain rate. Dip varies.
Dip of fault within the central bend
Throw rate of the bend (relative to the main fault)
0
1
2
4
30
60
90
120
150
40
50
70

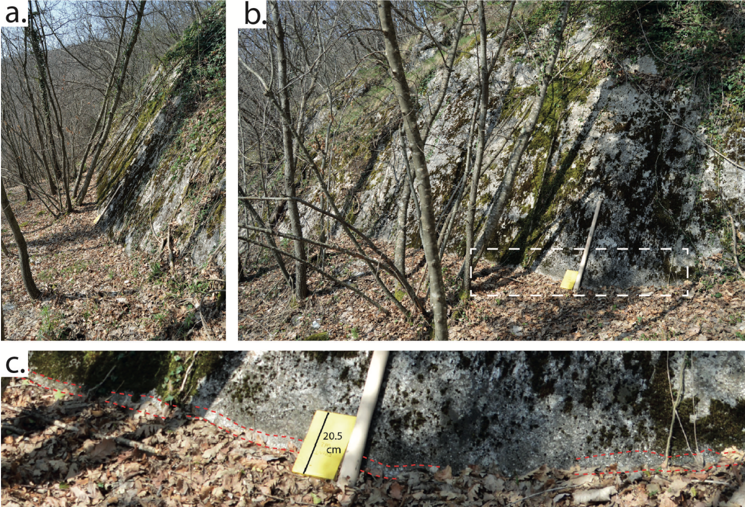
a.
b.
c.
20.5
cm

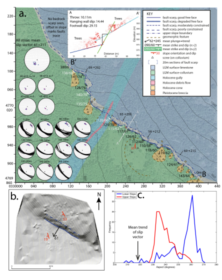

a.
No bedrock scarp seen offset in slope marks faults trace
All striae, mean slip vector: 61→211
Throw: 10.11m
Hanging wall dip: 14.44
Footwall dip: 29.15
Trees
Distance (m)
Elevation (m)
KEY
fault scarp, good free face
fault scarp, degraded free face
fault scarp, moderately constrained
fault scarp, poorly constrained
upper slope boundary
geomorphic feature
62→245 mean plunge→trend
090/60 mean strike and dip (n>2)
090/60 mean strike and dip (n<2)
30 slope orientation and dip
scree (on colluvium)
20m sections of fault scarp
LGM surface-limestone
LGM surface-colluvium
Holocene gully
Holocene debris flow
Holocene cone
Pleistocene breccia
b.
N
c.
Lower Slope
Upper Slope
Frequency
Mean trend of slip vector
Aspect (degrees)

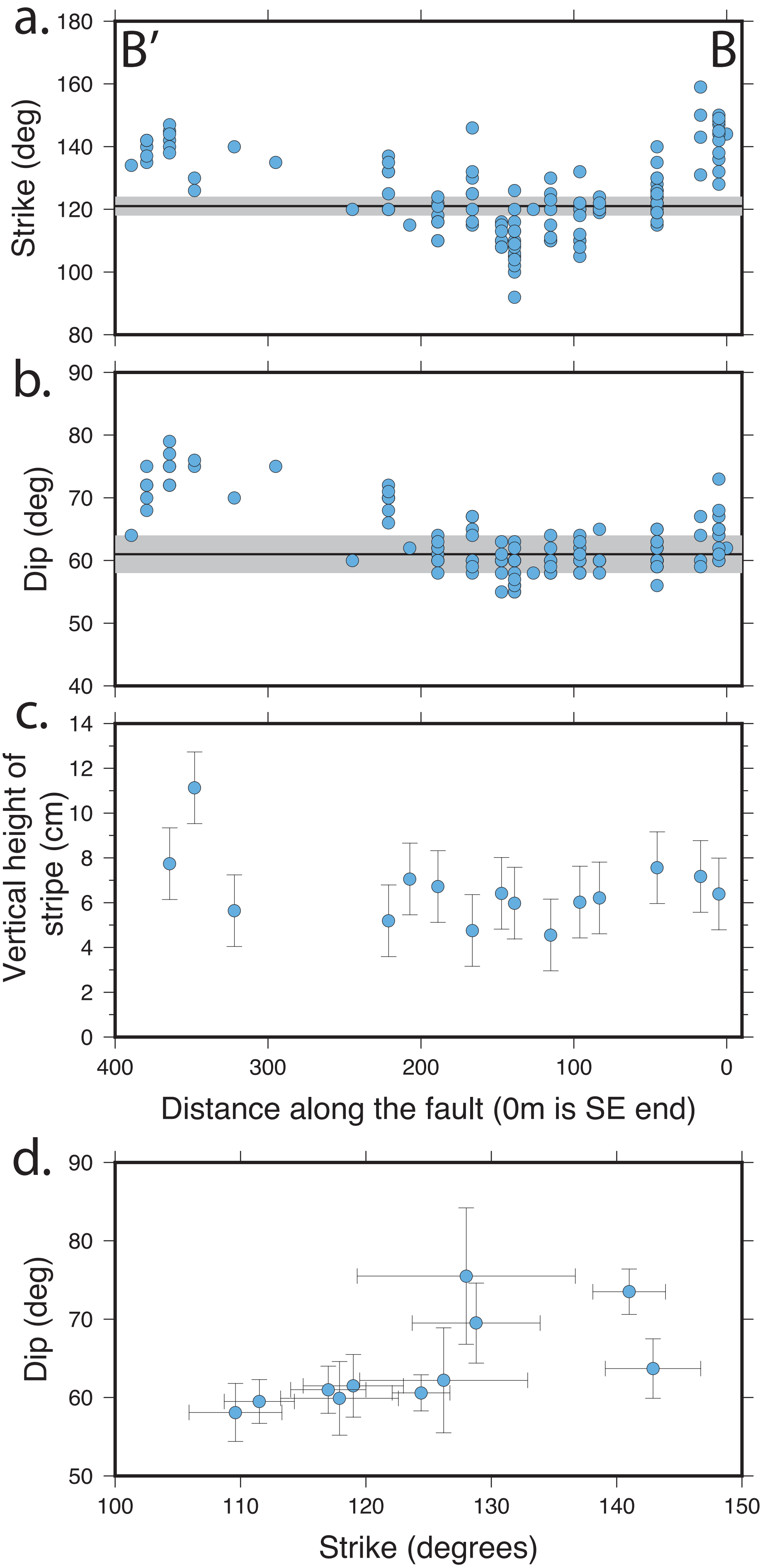
a.
B′
B
Strike (deg)
180
160
140
120
100
80
b.
Dip (deg)
90
80
70
60
50
40
c.
Vertical height of stripe (cm)
14
12
10
8
6
4
2
0
400
300
200
100
0
Distance along the fault (0m is SE end)
d.
Dip (deg)
90
80
70
60
50
100
110
120
130
140
150
Strike (degrees)

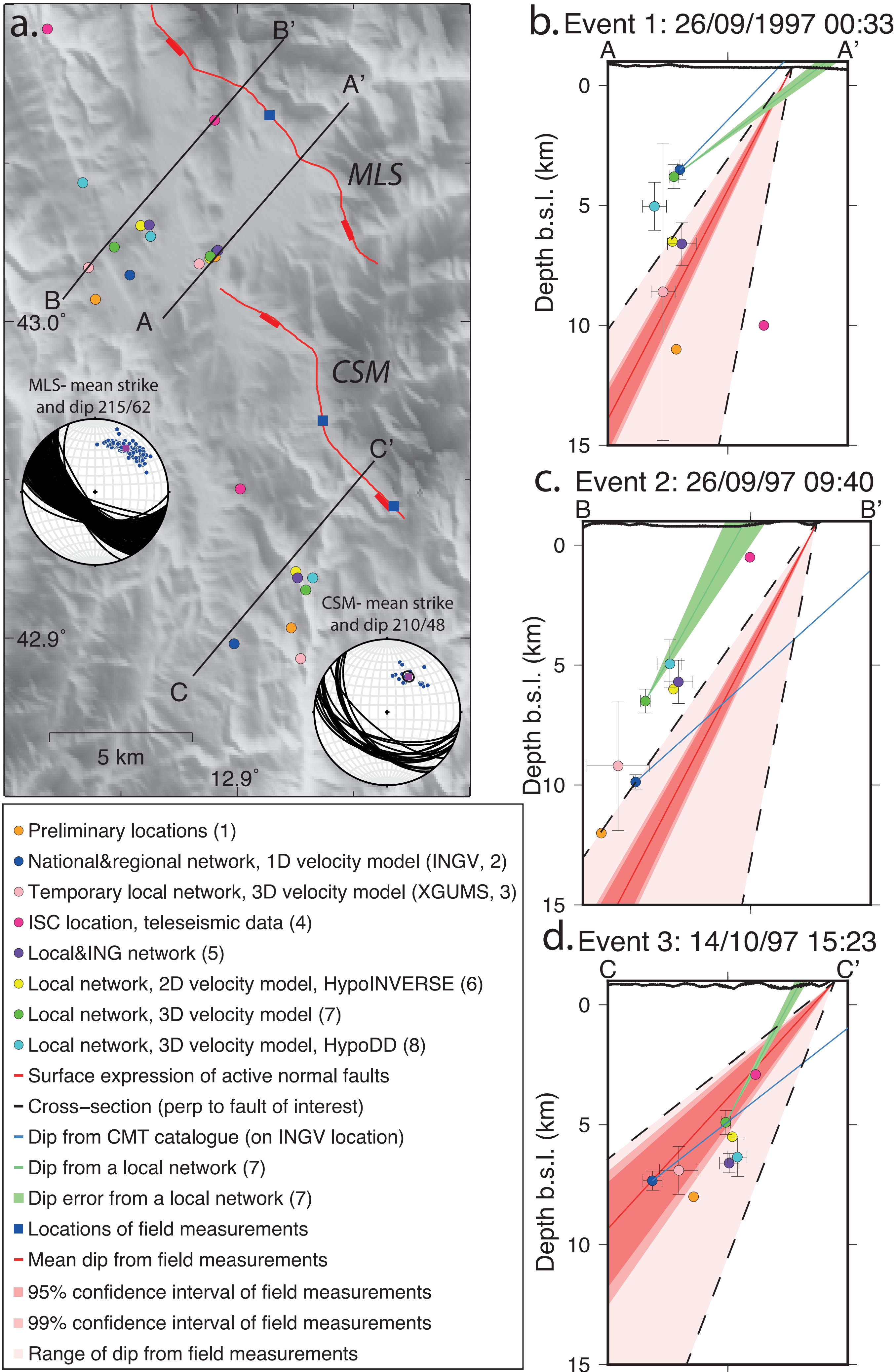

a.
B'
A'
MLS
B
A
43.0°
CSM
MLS- mean strike and dip 215/62
C'
CSM- mean strike and dip 210/48
42.9°
C
5 km
12.9°
Preliminary locations (1)
National&regional network, 1D velocity model (INGV, 2)
Temporary local network, 3D velocity model (XGUMS, 3)
ISC location, teleseismic data (4)
Local&ING network (5)
Local network, 2D velocity model, HypoINVERSE (6)
Local network, 3D velocity model (7)
Local network, 3D velocity model, HypoDD (8)
Surface expression of active normal faults
Cross–section (perp to fault of interest)
Dip from CMT catalogue (on INGV location)
Dip from a local network (7)
Dip error from a local network (7)
Locations of field measurements
Mean dip from field measurements
95% confidence interval of field measurements
99% confidence interval of field measurements
Range of dip from field measurements
b. Event 1: 26/09/1997 00:33
A
A'
Depth b.s.l. (km)
0
5
10
15
c. Event 2: 26/09/97 09:40
B
B'
Depth b.s.l. (km)
0
5
10
15
d. Event 3: 14/10/97 15:23
C
C'
Depth b.s.l. (km)
0
5
10
15

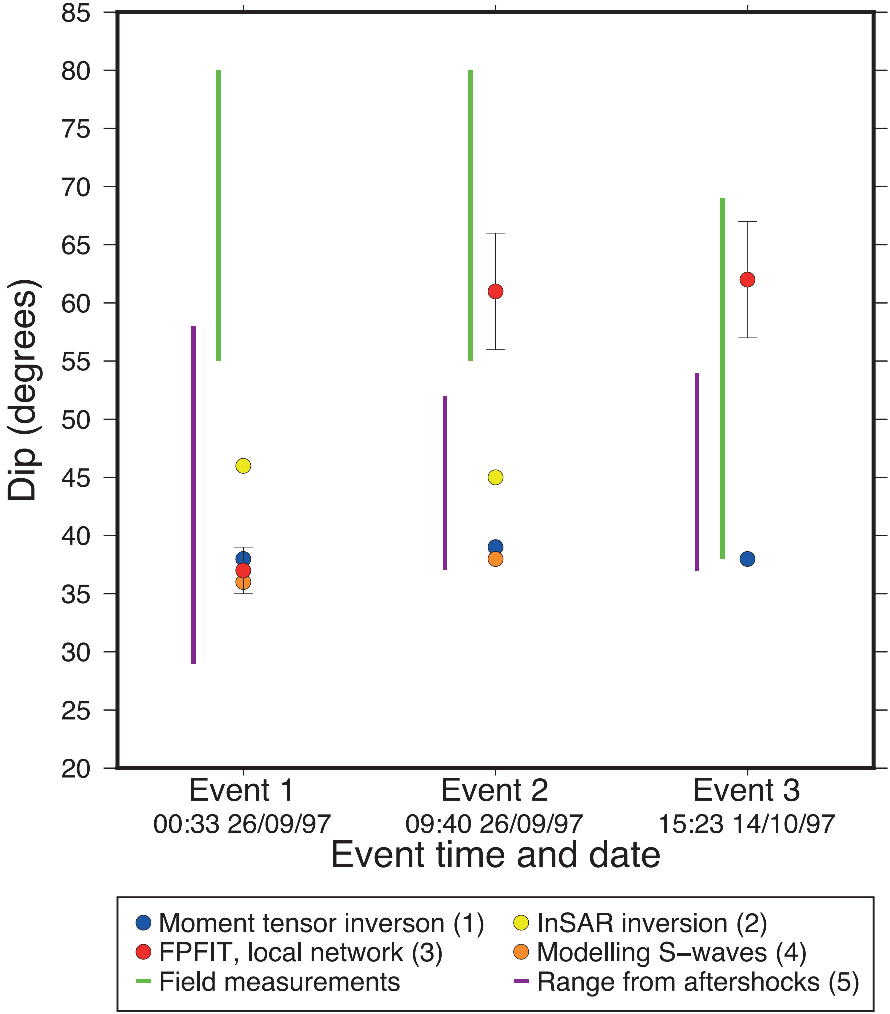

85
80
75
70
65
60
55
50
45
40
35
30
25
20
Dip (degrees)
Event 1
00:33 26/09/97
Event 2
09:40 26/09/97
Event 3
15:23 14/10/97
Event time and date
Moment tensor inverson (1)
InSAR inversion (2)
FPFIT, local network (3)
Modelling S−waves (4)
Field measurements
Range from aftershocks (5)